ATP-EMTP Simulation of Power Transformers for Detecting Winding Faults Using Sweep Frequency Response Analysis

Mehmet Salih Mamiş
Inonu University, Türkiye
Department of Electrical and Electronics Engineering
Engineering Faculty, 44280, Malatya
mehmet.mamis@inonu.edu.tr

İlker Arı
Siirt University, Türkiye
Department of Motor Vehicles and Transportation Technologies
Vocational School of Technical Sciences, 56100, Siirt
ilker.ari@siirt.edu.tr

Cemal Keleş
Inonu University, Türkiye
Department of Electrical and Electronics Engineering
Engineering Faculty, 44280, Malatya
cemal.keles@inonu.edu.tr

Müslüm Arkan
Inonu University, Türkiye
Department of Electrical and Electronics Engineering
Engineering Faculty, 44280, Malatya
muslum.arkan@inonu.edu.tr

Abstract- *Transformers are essential components in power transmission and distribution. Power transformers are necessary on both sides of transmission lines to facilitate energy transfer over long distances, while distribution transformers are utilized for energy distribution near power generation points. Despite their critical role in power systems, EMTP-based simulation programs lack an adequate model for transformer transient behavior. This study establishes the theoretical foundation for developing a transient model of a power transformer that is compatible with the ATP-EMTP program, using winding characteristics obtained through Sweep Frequency Response Analysis (SFRA). Additionally, a proposal is presented for incorporating frequency dependence into the transient model.*

Keywords*: Transformer, Modelling, SFRA, ATP-EMTP simulation, Faults.*

1 Introduction

Transformer faults pose a significant challenge to the continuous transmission of energy to consumers. Lightning strikes, short circuits, and switching events can lead to insulation deformation, arc formation, and turn-to-turn contact, resulting in solid short circuit faults. If these faults are not identified and addressed promptly, they can cause complete failure of the transformer windings, leading to prolonged power outages. Winding faults initially manifest as weak arcing faults, which can evolve into permanent solid short circuit faults over time. The high heat generated from the short circuit causes the transformer to heat up rapidly, potentially resulting in complete winding damage due to the inability to dissipate excess heat, and may even cause the transformer to explode due to high pressure. Therefore, detecting

internal arc faults in transformers is critical. The most crucial condition for a rapid response to malfunctions is the accurate prediction of the fault's initiation and type. Currently, faults are detected using the Buchholz relay, which senses hydrogen gas generated during the arc in the oil used for cooling in oil-cooled transformers. However, this process relies on chemical dissolution and can introduce delays, risking damage to the windings. Similarly, differential protection based on RMS current does not respond quickly to arc faults.

The literature review indicates that recent studies on identifying transformer winding faults have particularly focused on methods based on sweep frequency response analysis (SFRA) [1-5]. FRA can be categorized into two types: low voltage impulse (LVI) and sweep frequency response analysis (SFRA). In the SFRA method, the frequency response of the transformer is typically obtained through connections made at the transformer terminals using the SFRA instrument. By analyzing changes in this frequency response, it is possible to identify faults between the windings in the transformer using various techniques. Most of these studies conduct fault detection after the transformer has been taken offline, although the method has also been adapted for online fault detection [3].

This paper utilizes ATP-EMTP RLC electrical modeling. To perform a transient analysis of the transformer, a high-frequency model is required. Low-frequency transformer models are inadequate for transient analysis due to the distributed parameter structure of the windings and the exclusion of capacitance effects. To create the circuit model of the transformer in the ATP-EMTP program, the high-frequency parameters of the transformer must be known. For this purpose, the parameters of the transformers to be used in the laboratory will be determined through the FRA analysis method. This method is well-suited for obtaining the transformer's transient high-frequency model and is frequently employed [1-5].

Transformer RLC sequential circuits are derived from the SFRA spectrum. The transformer terminal voltage and currents are obtained by positioning the arc model between the points corresponding to the windings where the arc develops in ATP-EMTP. The arc model is implemented in ATPDraw using the MODELS language [6]. It consists of a MODELS block that takes the arc current as input and calculates the appropriate arc resistance, which is provided by the variable TACS resistor [7].

2 Modelling of Power Transformers for Transient Simulations

A power transformer ladder network model is formed by connecting multiple sections in sequence, each defined by lumped parameters R, L, and C. The equivalent circuit for the transformer is shown in Fig. 1. This figure illustrates a double ladder network model that encompasses both primary (high-voltage side) and secondary (low-voltage side) windings. Conversely, a single-ladder network model represents only one side of the transformer, either high-voltage or low-voltage. Each section represents a disc in the equivalent circuit, and the number of discs in the transformer windings dictates the number of sections in the model. The lumped parameters R_s, L_s, C_s, C_g, and C_{HL} correspond to the series resistance, self-inductance, series capacitance, shunt (ground) capacitance, and the capacitance between the high-voltage and low-voltage windings of the transformer, respectively. These parameters can be estimated or calculated based on winding design details, such as the geometry and physical properties of the transformer, or by using previously measured data. Methods like the Finite Element Method (FEM), analytical approaches, and terminal-based measurements are employed to calculate these model parameters. While transformer parameters are typically distributed like those in transmission lines, ladder circuits composed of lumped parameters have been

proposed for transformer modeling. Since a distributed model suitable for state-space analysis of transformer windings is not available, a lumped parameter model using ladder circuits needs to be utilized in ATP-EMTP simulations of the transformer winding.

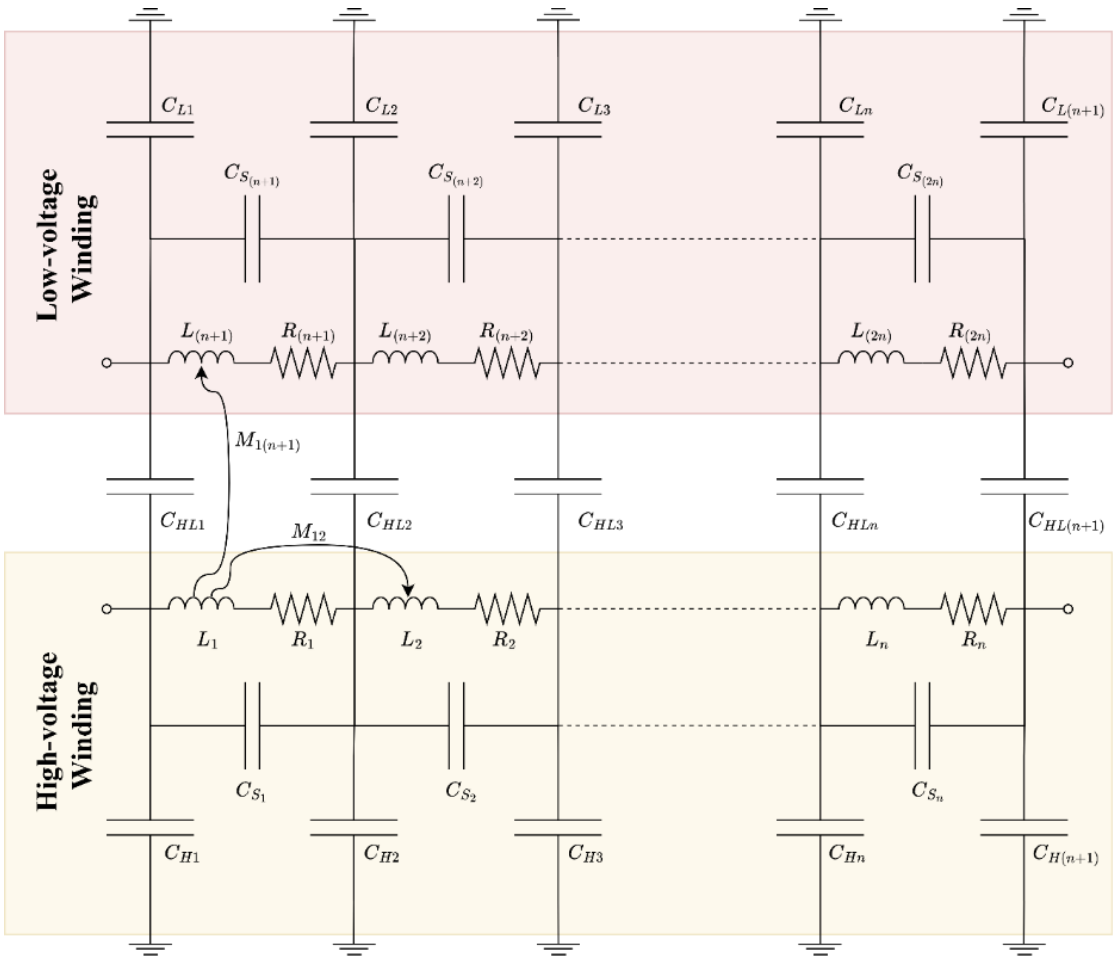


Figure 1. Equivalent circuit of the double ladder network for the power transformer winding.

2.1. Series Resistance of a Winding

The following equations are used to calculate the series resistance value (R_s) of a disc-type winding.

$$R_s = R_{s1}\varsigma_{ir} \tag{1}$$

In this equation, ς_{ir} represents the circumference of the conductor's resistance, $\varsigma_{ir} = 2\pi r$ and

$$R_{s1} = \frac{1}{2(h+w)}\sqrt{\frac{\pi f \mu}{\sigma}} \quad (\Omega/m) \tag{2}$$

In the given equation, h, w, μ, σ, and f represent the winding height, winding width, permeability, conductivity, and frequency, respectively. The conductivity matrix G is

calculated as follows.

$$G = 2\pi f C_s \tan\delta \tag{3}$$

Here, C_s represents the series capacitance, while $tan\delta$ denotes the insulation dissipation factor [8].

2.2. Self and Mutual Inductance of a Winding

The following equations are used to calculate the self and mutual inductance between turns in a disc-type winding [9].

$$L_{km} = \mu_0 N_k N_m \sqrt{d_1 d_2}\,\frac{2}{k}\left[\left(1-\frac{k^2}{2}\right)M(k) - E(k)\right] \tag{4}$$

where M in the above equation is

$$M = \sqrt{\frac{4d_1 d_2}{d_3^2 + (d_1 + d_2)^2}} \tag{5}$$

Here, L_{km} represents the mutual inductance between the k and m discs. μ_o is the magnetic permeability of the medium and N_m denote the number of sections k and m, while d_1 and d_2 represent the mean radii of the discs, and d_3 indicates the axial distance between the discs as shown in Fig. 2. When k=m, the self-inductance is calculated as d_3 = 0.02235(h+w). M and E represent elliptic integrals of the first and second kind. For the L_{km} matrix, the diagonal elements represent the self-inductance, while the off-diagonal elements represent the mutual inductance between the discs. Since the mean radii of the sections are the same, the values of d_1 and d_2 are equal in this calculation [10].

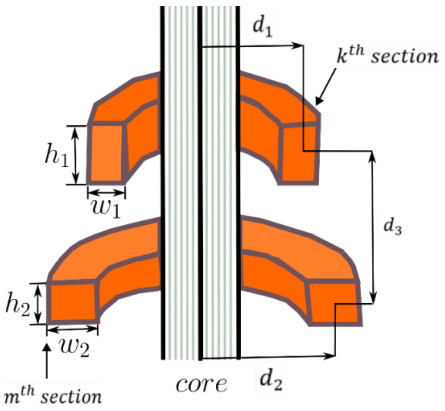


Figure 2. Dimensions of winding discs [9].

2.3. Calculating the Series Capacitance of a Winding

To determine the series capacitance value based on the transformer winding structure, we calculate two types of capacitances: the capacitance between conductors in the same disc (C_t) and the capacitance between conductors in adjacent discs, known as the inter-disc capacitance (C_d). The structure of a single-phase disc-type winding is illustrated in Figure 3. The

capacitance between conductors in the same disc (between two windings) is calculated as follows [8,12]:

$$C_t = \frac{2\pi\varepsilon_r\varepsilon_0 d_w}{\ln\frac{b_1}{b_2}} \tag{6}$$

In this equation, b_1 represents the inner radius of the outer conductor, b_2 represents the outer radius of the inner conductor, and d_w represents the length of the conductor. ε_0 is the permittivity of free space, and ε_r is the relative permittivity of the insulation paper between the inner and outer conductors, where typically $\varepsilon_r = 3.85$ for paper insulation.

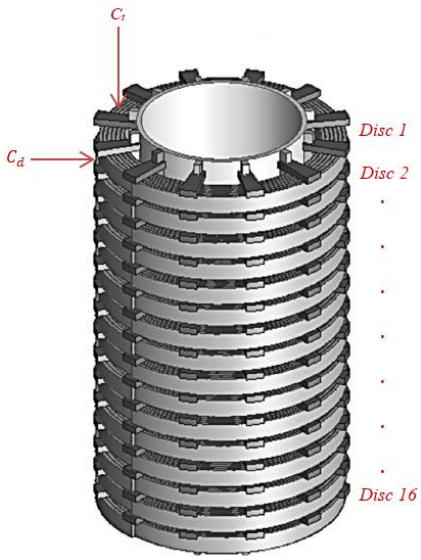


Figure 3. Structure of single-phase disc-type winding [11].

The equations given below are used to calculate the capacitance (C_d) between any two discs [10].

$$C_d = \varepsilon\frac{S}{d} \tag{7}$$

$$S = \pi\left(\left(\frac{d_o}{2}\right)^2 - \left(\frac{d_i}{2}\right)^2\right) \tag{8}$$

$$S = \pi\left(\frac{d_o^2}{4} - \frac{d_i^2}{4}\right) \tag{9}$$

where $\varepsilon = \varepsilon_r\varepsilon_0$.

$$C_d = \varepsilon_r\varepsilon_0\pi\frac{d_o'^2 - d_i'^2}{4d} \tag{10}$$

In the equations above, $d_i' = d_i - d$ and $d_o' = d_o + d$. Here, d, d_o, and d_i represent the distance between the windings, the outer diameter of the winding, and the inner diameter of the winding, respectively. S is the surface area of the disc. Based on the transformer capacitance equivalent circuit shown in Figure 4, the following equations are used to calculate the total value of C_t and C_d :

$$C_{t\,total} = \frac{1}{\frac{1}{C_{t1}} + \frac{1}{C_{t2}} + \frac{1}{C_{t3}} + \frac{1}{C_{tn}}} \tag{11}$$

$$C_{d\,total} = C_{d1} + C_{d2} + C_{d3} + C_{dn} \tag{12}$$

Using Figure 4 and equations (11) and (12), the capacitance value of the transformer winding for a disc can be calculated as C_d+C_t. However, the following equation is used to determine the total series capacitance value of the winding.

$$C_s = \frac{1}{N_d}\left(\frac{C_t}{mt} + 4C_{dt}\right) \tag{13}$$

$$C_{dt} = \frac{(mt-1)(2mt-1)}{6mt} C_d \tag{14}$$

Here, mt represents the number of turns per disc. C_{dt} is calculated based on the capacitance between the discs. In addition to C_t and C_d, the disc model of the transformer winding also includes a capacitance to ground, referred to as C_g. The value of C_g is calculated using the formula provided below [10]:

$$C_g = \frac{2\pi\varepsilon_r\varepsilon_0 d_w}{\ln\left(\frac{d_i}{d_o}\right)} \tag{15}$$

The voltage distribution factor (α) is crucial for analyzing voltage distributions in transformer windings. The formula for the voltage distribution factor is as follows [13]:

$$\alpha = \sqrt{C_g / C_s} \tag{16}$$

The value of a given parameter in the formula should be kept small; otherwise, the insulation of the transformer may be at risk. Therefore, this factor is important for the design of winding insulation in transformers.

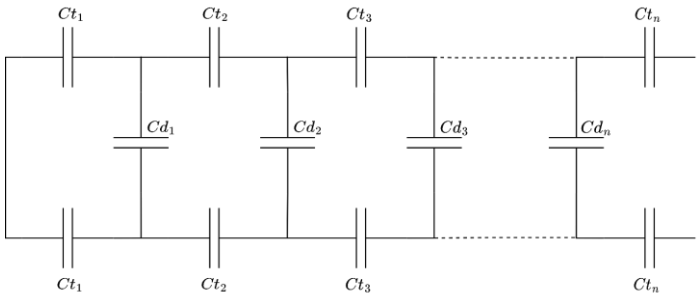


Figure 4. Equivalent circuit of transformer winding capacitance

2.4. Penetration Depth and Ferromagnetic Effects

The relationship between penetration and the iron core determines how electromagnetic waves, or magnetic fields, propagate in ferromagnetic materials such as iron. Ferromagnetic materials exhibit high magnetic permeability, resulting in a superficial penetration depth. Consequently, magnetic fields penetrate only to the surface region, not reaching the deeper layers of the iron core. This phenomenon, which develops in the surface region, is known as the skin effect. As the frequency increases, the magnetic flux becomes concentrated near the surface, and the penetration depth becomes significantly smaller than the physical dimensions of the iron core. Under these conditions, the inner regions of the core become ineffective and do not contribute to the magnetic flux. Therefore, the magnetization within the iron core can be neglected at high frequencies. This relationship is crucial for transformer design and understanding the effects of core losses in high-frequency applications. The penetration depth is expressed as follows [14,15].

$$\delta = \sqrt{\frac{2}{\omega \mu \sigma}} \tag{17}$$

In transformer modeling studies, assumptions have been made that the core effect can be neglected, especially at frequencies above 10 kHz [14].

3 Application and Results

Frequency Response Analysis (FRA) is a powerful diagnostic technique used to evaluate the mechanical integrity of transformers. FRA involves measuring the impedance or transfer function across a broad frequency range to identify structural changes in the transformer windings and core. Given that the high-frequency behavior of the transformer is crucial for FRA testing, a suitable high-frequency model is essential for accurately interpreting the results. In FRA, alterations in the transformer's internal structure result in shifts in resonance points or changes in magnitude within the frequency response. A high-frequency model helps to precisely detect these variations.

FRA results are analyzed across three regions of frequency:

- Low Frequency Region (20 Hz - 2 kHz): Core saturation and magnetic circuitry effects are most significant.
- Medium Frequency Region (2 kHz - 20 kHz): Inductive and capacitive interactions between windings dominate.
- High Frequency Region (20 kHz - 2 MHz): Parasitic capacitances become critical, revealing internal resonances within the transformer structure.

Various approaches exist for modeling the high-frequency behavior of power transformers, with circuit-based models, field-based models, and mixed (hybrid) models being the most common. Among them are Multiconductor Transmission Lines (MTLs), Circular Multiconductor Transmission Lines (CMTLs), ladder networks, and hybrid models (MTL-ladder networks) as outlined in the literature [17]. While MTLs and CMTLs focus on winding-based models, this study employs a disc-based ladder network model.

The test system constructed in laboratory is shown in Fig. 5. 50 kVA 10 kV/400 V transformer is used in the test. SFRA tests are carried out using FRAX 101. Connection diagram for transformer winding self-impedance measurement is shown in Fig. 6. The results

obtained with this test are used to determine HV and LV side series capacitance between windings. Figures 7 and 8 illustrate SFRA graphics taken from FRAX 101 instrument.



Figure 5. Laboratory setup for transformer SFRA tests.

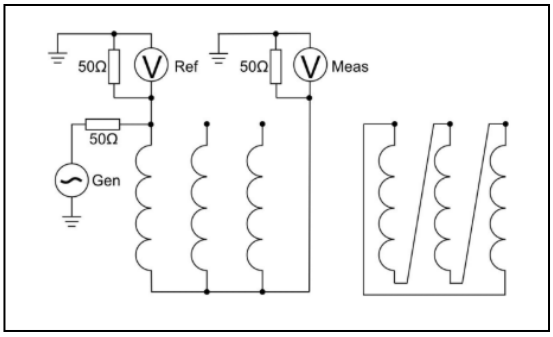


Figure 6. Connection diagram for transformer winding self-impedance measurement.

It is possible to obtain transformer self-capacitances using the impedance and angle graphs in Figures 7 and 8. To do this, first determine the inductance value by considering the impedance value at the lowest frequency (e.g., 20 Hz, the lowest measurement frequency). Then, the value of *C* at the resonant frequency is calculated using the following equation:

$$f = \frac{1}{2\pi\sqrt{LC}} \tag{18}$$

Since Figure 7 shows the average impedance value for the HV side phases at 20 Hz as 12804.3 **Ω** and the angle is 72°, the inductance of $L = \frac{|Z|\sin(\emptyset)}{2\pi f}$ =96.91 H is found. The resonant frequency is 1025 Hz. In this case, the winding self-capacitance of C_{sH}=0.25 nF is obtained for the HV side from Eqn. (18).

A similar procedure is repeated for the LV side. Considering Fig. 8, the average impedance value for the three phases at *f*=20 Hz is 65 **Ω** and the angle is 74°, resulting inductance of 0.497 H. The resonant frequency is 437 Hz. In this case, the winding self-capacitance of C_{sL}=0.27 µF is determined for the LV side.

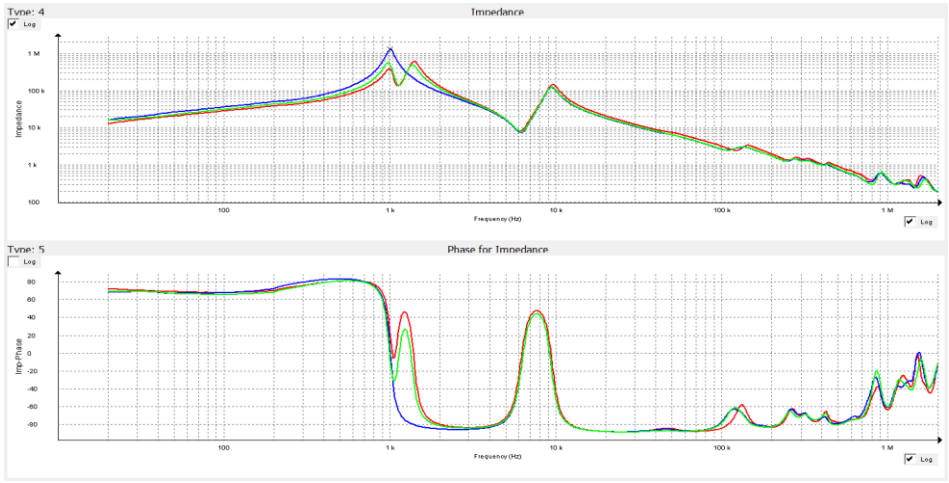


Figure 7. HV side SFRA impedance and phase measurements.

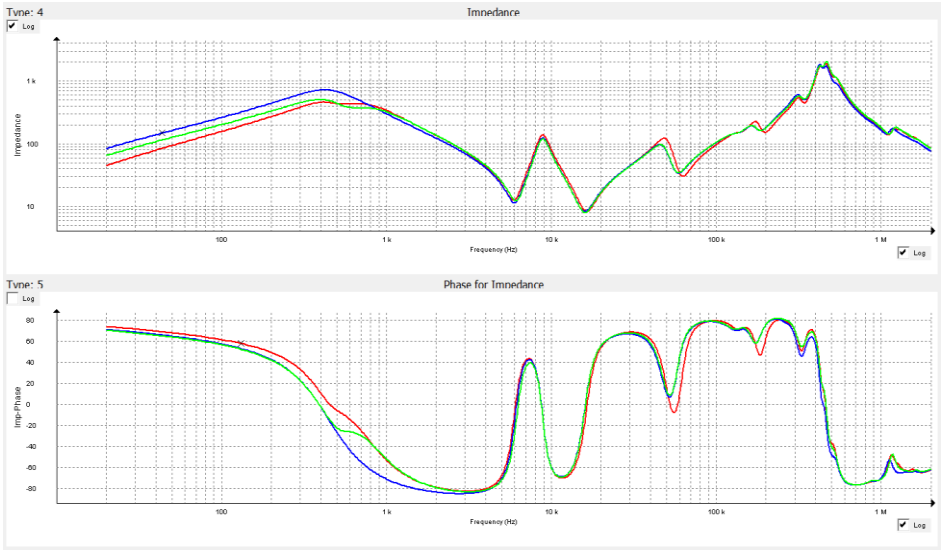


Figure 8. LV side SFRA impedance and phase measurements.

To determine the capacitance between the high-voltage (HV) and low-voltage (LV) windings, the probes of the SFRA device are connected as shown in Figure 9. The resulting SFRA graph is presented in Figure 10. Considering the measuring configuration, the impedance at lowest frequency (20 Hz) is is 8.57 MΩ and the capacitance is determined to be 0.928 pF.

To determine the capacitance between the HV winding and ground, as well as the LV winding and ground, the SFRA device is connected as shown in Figure 9, with a measuring probe connected to the ground. The resulting SFRA graph is shown in Figure 11. Considering the measuring configuration, the impedance at lowest frequency (20 Hz) is 52.3 MΩ and the capacitance is determined to be $C_H = C_L$ =152 pF.

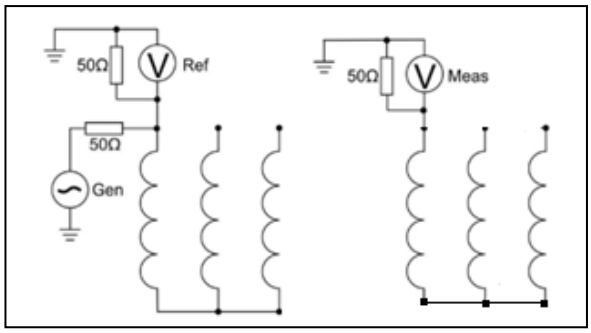


Figure 9. Connection diagram for transformer winding HV-LV mutual capacitance measurement.

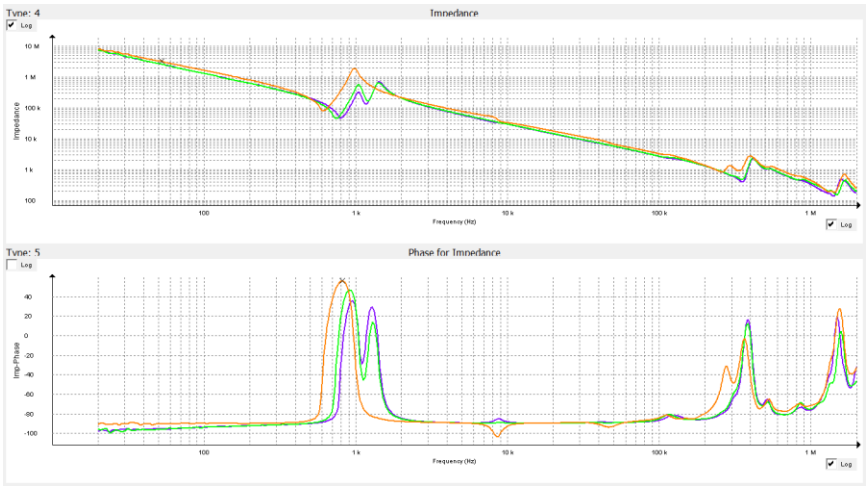


Figure 10. SFRA impedance and phase measurements for HV-LV mutual capacitance determination.

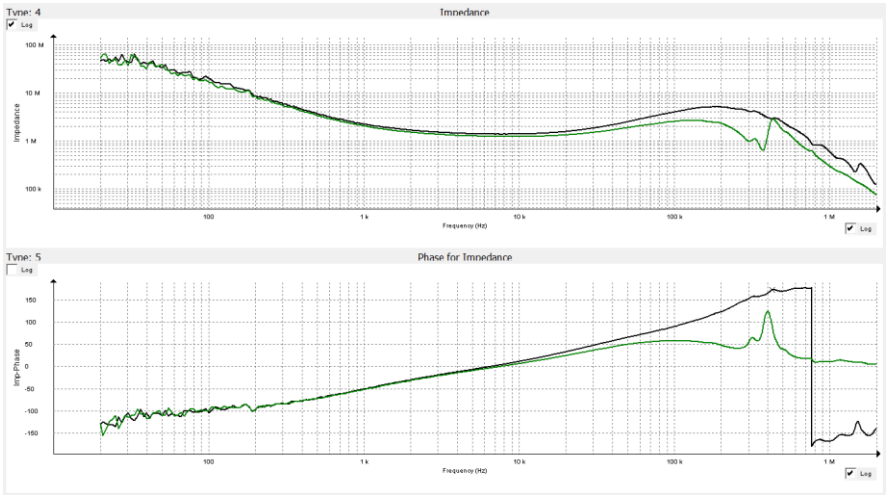


Figure 11. HV-Ground connection SFRA impedance and phase measurements for capacitance to ground determination.

The connection diagram for measuring phase-to-phase mutual capacitance in transformer windings is the same as that shown in Fig. 9. However, the measuring probe is connected to one of the phases on the same side, with the neutral point of each winding isolated. On the LV side, measurements are taken between phases a-b, b-c, and a-c, while on the HV side, measurements are taken between phases A-B, B-C, and A-C. The SFRA impedance and phase measurements are presented in Fig. 12. The red, green, and black curves correspond to the HV winding, while the other lines represent the LV side measurements.

For the HV winding, the impedance is 30356 Ω at 20 Hz, and the phase angle is 72° at that frequency. The calculated mutual inductance is 229.7 H. The resonant frequency is 1100 Hz, which results in the mutual capacitance between the phase windings as 91.1 pF. Similarly, for the LV winding, the impedance is 130 Ω at 20 Hz, and the phase angle is also 72°. The resonant frequency is 502 Hz. Based on these values, the mutual capacitance of the LV side windings is calculated to be 0.102 μF.

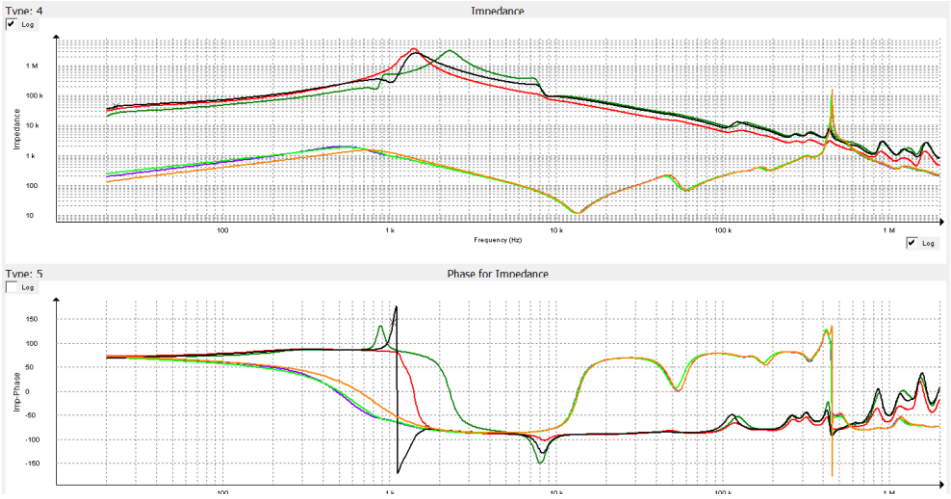


Figure 12. HV side A-B, B-C, A-C and LV side a-b, b-c, a-c SFRA impedance and phase measurements.

The ATP-EMTP simulation of phase A of the transformer is presented in Fig. 13. Ten ladder circuits are used to represent the transformer. The transformer is fed through a 30 km transmission line. The voltage and current profiles at the sending and receiving ends of the transmission line obtained with the ATP-EMTP are shown in Fig. 14.

In the second case, the arc model is connected to the 5th section to ground, and transient voltages are computed. The ATP-EMTP arc model is shown in Fig. 15. It is assumed that the arc initiates at *(t* =2) ms. The transmission line sending-end voltage and the voltage at the transformer terminal are shown in Fig. 16. It can be observed from the figure that high-frequency components are generated in the sending-end voltage of the transmission line. Additionally, the sinusoidal shape of the voltage at the transformer terminals deforms due to the generated arc. This transient phenomenon can be used for fault identification inside a power transformer.

While there are many proposals for expressing the frequency dependence of line parameters in EMTP programs for transmission lines, the model that comprehensively incorporates

frequency dependence for transformers does not exist. It is estimated that transformer series impedance can be expressed as frequency-dependent using the methods used for transmission lines. The RL circuit model may be used, as referenced in [20], to express the frequency dependence of line series impedance. Good results were obtained by integrating this circuit into π-sections for transmission lines. The number of RL branches can be increased if necessary to achieve the desired accuracy. Using this model in the transformer equivalent circuit, it is considered possible to express frequency dependence.

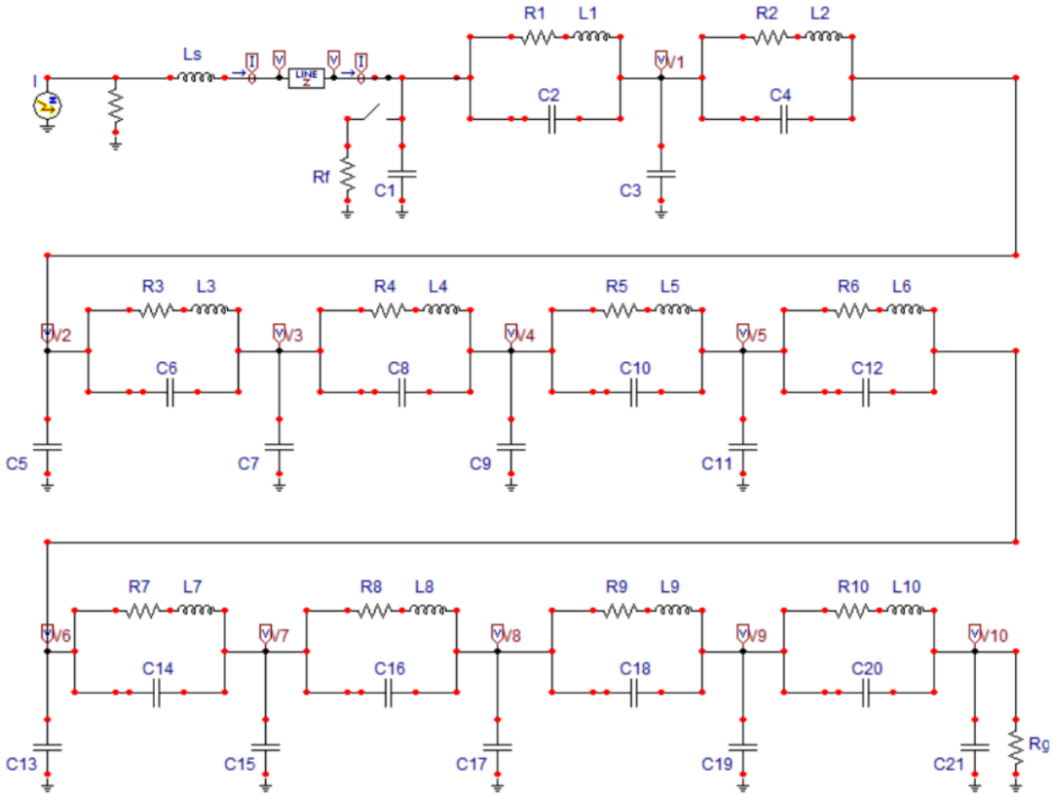


Figure 13. ATP-EMTP simulation of a lightning strike on a transmission line connected to the transformer.

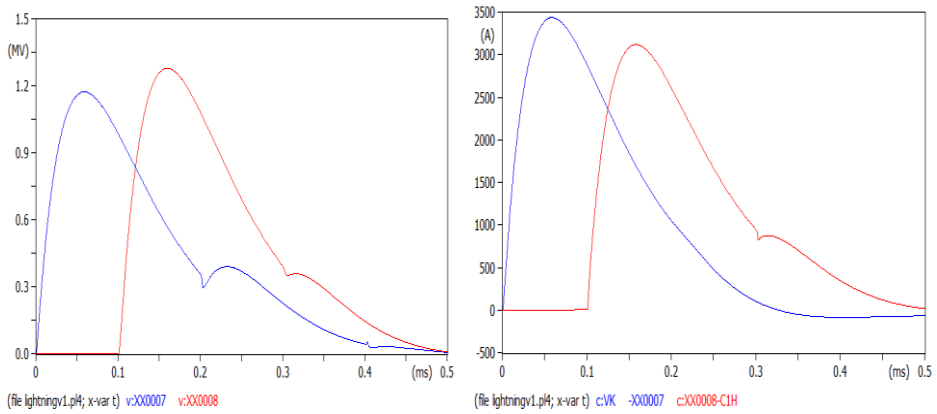


Figure 14. The voltage and current profiles of the sending- and receiving-end of the transmission line obtained with the ATP-EMTP (Blue: Sending-end of TL, Red: Transformer terminal)

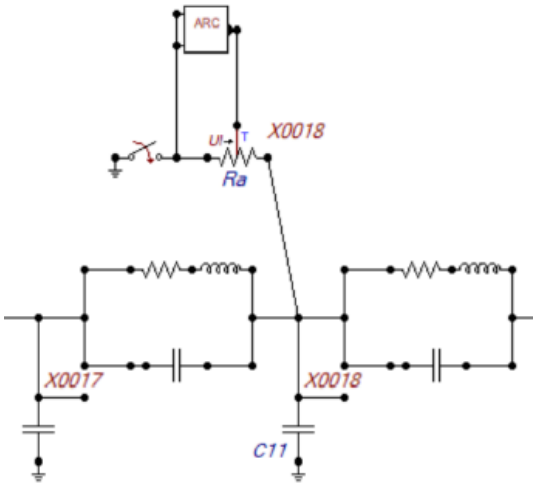


Figure 15. Arc model at node 15.

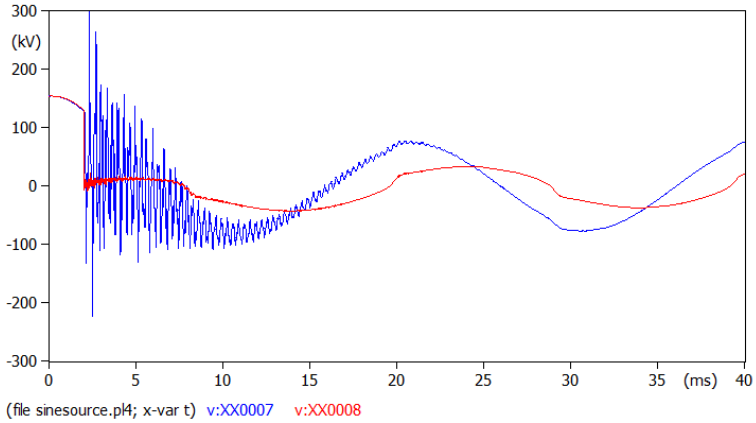


Figure 16. The voltages at the transmission line sending-end (blue) and the transformer terminal (red).

4 Conclusion

Transient analysis and the investigation of transformer internal structure-related fault conditions require a model that represents the transformer across a wide spectrum, including high frequencies. This study utilizes magnitude and angle plots obtained from SFRA measurements to investigate how the transformer transient equivalent circuit should be constructed, and the corresponding results are presented. Including the frequency dependence due to the skin effect will also contribute to the model.

5 Acknowledgement

This study was supported by the Scientific and Technological Research Council of Turkey (TUBITAK) under Grant Number 123E658 and the Research Fund of Inonu University, Project Number FDP-2024-3702. The authors thank TUBITAK and the Research Fund of Inonu University for their support.

6 References

[1] Senobari, R. K., Sadeh, J., Borsi, H.: *Frequency Response Analysis (FRA) of Transformers as a Tool for Fault Detection and Location: A Review*, Electric Power Systems Research, (2018), 155, pp.172-183.

[2] Moradzadeh, A., Pourhossein, K.: *Early Detection of Turn-to-Turn Faults in Power Transformer Winding: an Experimental Study*, International Aegean Conference on Electrical Machines and Power Electronics (IEEE ACEMP) & 2019 International Conference on Optimization of Electrical and Electronic Equipment (OPTIM), (2019), pp. 199-204.

[3] Zhao, X., Yao, C., Zhou, Z., Li, C., Wang, X., Zhu, T., Abu-Siada, A.: *Experimental Evaluation of Transformer Internal Fault Detection Based on V–I Characteristics*, IEEE Transactions on Industrial Electronics, (2019). 67(5), pp.4108-4119.

[4] Yoon, Y., Son, Y., Cho, J., Jang, S., Kim, Y. G., Choi, S.: *High-Frequency Modeling of a Three-Winding Power Transformer using Sweep Frequency Response Analysis*, Energies, (2021), 14(13), 4009.

[5] Moradzadeh, A., Moayyed, H., Mohammadi-Ivatloo, B., Gharehpetian, G. B., Aguiar, A. P.: *Turn-to-Turn Short Circuit Fault Localization in Transformer Winding via Image Processing and Deep Learning Method*, IEEE Transactions on Industrial Informatics, (2022), vol. 18, no. 7, pp.4417-4426.

[6] Dubé L.: *Language Manual MODELS IN ATP*, 1996.

[7] Prikler, L., Hoidalen, HK.: *ATPDRAW manual Preliminary Release*, 2009.

[8] Popov, M., Gustavsen, B., Martinez-Velasco, JA.: *Electromagnetic Transients in Transformer and Rotating Machine Windings* (1st Ed.). Pennsylvania, USA, 2012.

[9] Wilcox, D. J., Hurley, W. G., Conlon, M.: *Calculation of self and mutual impedances between sections of transformer windings.* IEE Proceedings C: Generation Transmission and Distribution, (1989). 136(5), pp.308–314.

[10] Al-Ameri, S. M. A. N., Kamarudin, M. S., Yousof, M. F. M., Salem, A. A., Banakhr, F. A., Mosaad, M. I., Abu-Siada, A.: *Understanding the Influence of Power Transformer Faults on the Frequency Response Signature Using Simulation Analysis and Statistical Indicators*, IEEE Access, (2021). 9, pp.70935–70947.

[11] Jaarsveld, B. J. Van.: *Wide band modelling of an air-core power transformer winding* (Master's thesis). Retrieved from https://scholar.sun.ac.za/items/5a96304a-26f7-4052-8898-d29338327623, 2013.

[12] Kulkarni, S. V.; Khaparde, S. A.: *Transformer Engineering: Design and Practice* (1st ed.). New York, USA, 2004.

[13] Samal, M., Lakshmi Prasanna, K., Mishra, P., Mondal, M.: *Accurate Estimation of Transformer Winding Capacitances and Voltage Distribution Factor Using Driving Point Impedance Measurements,* IEEE Access, (2024). 12(September), pp.133670–133684.

[14] Olivares, J. C., Cañedo, J., Moreno, P., Driesen, J., Escarela, R., Palanivasagam, S.: *Experimental Study to Reduce the Distribution-Transformers Stray Losses Using Electromagnetic Shields*, Electric Power Systems Research, (2002), 63(1), pp.1–7.

[15] Penabad-Durana, P., Lopez-Fernandez, X. M., Turowski, J.: *3D Non-Linear Magneto-Thermal Behavior on Transformer Covers*, Electric Power Systems Research, (2015), 121, pp.333–340.

[16] Abeywickrama, N., Serdyuk, Y. V., Gubanski, S. M.: *High-Frequency Modeling of Power Transformers for use in Frequency Response Analysis (FRA),* IEEE Transactions on Power Delivery, (2008), 23(4), pp.2042–2049.

[17] Samal, M., Mondal, M.: *Power Transformer FRA Studies Using Ladder, Multi-Conductor Transmission Lines (MTL), Circular MTL, and Hybrid Winding Models*, 2023 IEEE 8th International Conference for Convergence in Technology, Lonavla, India, April 7-9., (2023), pp.1–6.

[18] Yiwei, F., Chenguo, Y., Jiangnan, L., Shoulong, D., Yu, L., Huangtong, L., Lisheng, Z.: *Equivalent Circuit Model and Experimental Validation of Transformer Windings Considering Long-Distance Conductor Effects and Frequency-Dependent Parameters*, IET Electric Power Applications, (2025). 19(1).

[19] Thein, M. M., Toda, H., Hikita, M., Ikeda, H., Haginomori, E., Koshiduka, T.: *Investigation of Transformer Model for TRV Calculation by Using Frequency Dependent Inductance Model*, Journal of International Council on Electrical Engineering, (2011). 1(2), pp.188–193.

[20] Pascoalato, T. F., de Araújo, A. R., Kurokawa, S., Pissolato Filho, J.: *Alternative method to include the frequency-effect on transmission line parameters via state-space representation*, International Journal of Electrical Power & Energy Systems, (2024), *155*, 109375.